Functionalized Tetrapodal Diazatriptycenes for Electrostatic Dipole Engineering in n-Type Organic Thin Film Transistors

Valentina Rohnacher, Frank S. Benneckendorf, Maybritt Münch, Eric Sauter, Andika Asyuda, Marc-Michael Barf, Jean-Nicolas Tisserant, Sabina Hillebrandt, Frank Rominger, Daniel Jänsch, Jan Freudenberg, Wolfgang Kowalsky, Wolfram Jaegermann, Uwe H. F. Bunz, Annemarie Pucci, Michael Zharnikov, and Klaus Müllen*

A diazatriptycene-based tetrapodal scaffold with thiol anchors enforces a nearly upright orientation of functional groups, introduced to its quinoxaline subunit, with respect to the substrate upon formation of self-assembled monolayers (SAMs). Substitution with electron-withdrawing fluorine and cyano as well as electron-rich dimethylamino substituents allows tuning of the molecular dipole and, consequently, of the work function of gold over a range of 1.0 eV (from 3.9 to 4.9 eV). The properties of the SAMs are comprehensively investigated by infrared reflection absorption spectroscopy, near edge X-ray absorption fine structure spectroscopy, and X-ray photo-electron spectroscopy. As prototypical examples for the high potential of the presented SAMs in devices, organic thin-film transistors are fabricated.

1. Introduction

Self-assembled monolayers (SAMs) are 2D ordered molecular assemblies,[1] which can be specifically tailored by the design of their constituents. The substrate or interface onto which the molecules are assembled can thus be customized for applications in sensors,[2] molecular machines[3] and switches,[4] electrochromism,[5] molecular,[6–8] and organic electronics.[9–11] In the latter field, SAMs are in particular used as active, semiconducting materials in organic field-effect transistors (OFETs) and as passive materials for the decoration of the gate dielectric, reducing charge trap states and operating voltages.[12–15] The wettability of the gate dielectric[16] and the morphology of the organic semiconductor[17] can be affected as well, improving charge carrier mobility and on/off ratio.[16] If coated onto electrodes, both oxidic[18] and metallic,[19] SAMs allow to tune the surface energies[18] and work functions (WF)[20] over a wide range relying on the inherent molecular dipole provided by the dipolar groups within the SAM-forming molecules.[21] Apart from the value of the respective dipole moment and the packing density of the SAM, the WF shift depends on the strength of the dipole, its direction, and its exact orientation relative to the electrode: a direction toward the interface reduces the WF and vice versa.[22] As to the exact orientation, the WF shift follows the $\cos(\theta)$ law, with θ being

V. Rohnacher, Dr. S. Hillebrandt,[+] Prof. A. Pucci
Kirchhoff Institute for Physics
Heidelberg University
Im Neuenheimer Feld 227, Heidelberg 69120, Germany

V. Rohnacher, Dr. F. S. Benneckendorf, Dr. M. Münch, Dr. M.-M. Barf, Dr. J.-N. Tisserant, Dr. S. Hillebrandt,[+] D. Jänsch, Dr. J. Freudenberg, Prof. W. Kowalsky, Prof. W. Jaegermann, Prof. A. Pucci
InnovationLab
Speyerer Straße 4, Heidelberg 69115, Germany

Dr. F. S. Benneckendorf, Dr. F. Rominger, D. Jänsch, Dr. J. Freudenberg, Prof. U. H. F. Bunz
Organisch-Chemisches Institut
Ruprecht-Karls-Universität Heidelberg
Im Neuenheimer Feld 270, Heidelberg 69120, Germany

Dr. M. Münch, Prof. W. Jaegermann
Material Science Department
Surface Science Division
Technische Universität Darmstadt
Otto-Berndt-Straße 3, Darmstadt 64287, Germany

Dr. E. Sauter, A. Asyuda, Prof. M. Zharnikov
Applied Physical Chemistry
Heidelberg University
Im Neuenheimer Feld 253, Heidelberg 69120, Germany

Dr. M.-M. Barf, Dr. J.-N. Tisserant, Prof. W. Kowalsky
Institut für Hochfrequenztechnik
Technische Universität Braunschweig
Schleinitzstraße 22, Braunschweig 38106, Germany

Prof. K. Müllen
Max-Planck Institute for Polymer Research
Ackermannweg 10, Mainz 55128, Germany
E-mail: muellen@mpip-mainz.mpg.de

[+]Present address: Organic Semiconductor Centre, SUPA, School of Physics and Astronomy, University of St Andrews, North Haugh KY16 9SS, UK

the angle between the direction of the dipole moment and surface normal (tilt angle), and is consequently maximal at upright orientation of the dipolar group ($\theta \approx 0°$).[22,23] Such an upright orientation is however difficult to achieve since the anchoring groups and character of the molecular backbone frequently enforce a tilted molecular orientation.[15] As a consequence it would be advantageous to create a system, which decouples the anchoring to the substrate from the decoration with versatile dipolar groups in nearly orthogonal orientation with respect to the substrate.

Such a decoupling can be achieved by employing conformationally rigid multipods, which control the spatial orientation and packing density of functional head groups upon self-assembly on solid supports by at least threefold covalent bonding—a topic reviewed recently.[24] Examples of surface-mountable tripods[25] include scaffolds with sp³-hybridzed carbon or silicon atoms,[25,26] e.g., tetraarylmethanes[27] and -silanes,[28] adamantanes,[29] spirobisfluorenes,[30] tris-NHC-functionalized benzenes,[31] transition metal complexes,[32] and triptycenes with their C_3 axis parallel to the surface normal.[33] Furthermore, bis(benzimidazolyl)pyridines, porphyrins,[34] and diruthenium complexes[35] were designed to realize fourfold anchors. Even adsorbates with more than four binding sites or even entirely physisorbed platforms[36] were reported. To modulate the WF of electrodes over a sufficiently broad range in a reliable and effective fashion such a scaffold has to 1) be compact enough to allow for a high dipole density, 2) ensure a nearly orthogonal orientation of the dipolar head groups with respect to the substrate, and 3) be easily functionalized to yield precursors of different dipolar strength. Regretfully, the multipods reported so far frequently fail to meet all the above criteria due to inhomogeneous bonding to the substrate resulting in stochastic molecular orientation (e.g., as reported for most tripodal systems), a large size of the molecular skeletons (≥tetrapods), and the necessity of time-consuming synthesis for any particular functionalization.

In this context, we recently designed a novel tetrapodal diazatriptycene (**DAT**), bearing four thiol-based anchoring groups, and demonstrated its capability to form well-defined and dense SAMs on Au(111) substrates while simultaneously ensuring a nearly upright orientation of its functional head
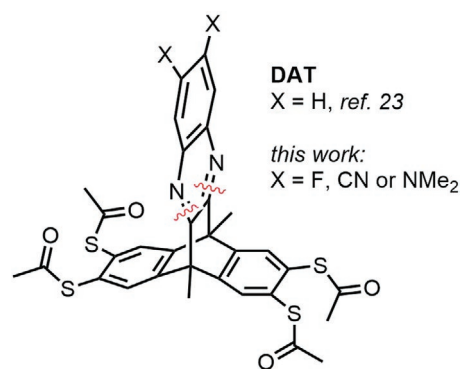
Figure 1. Molecular structure of DAT (X = H) depicting the condensation approach toward its quinoxaline subunit (red sinuous lines) and its dipolar derivatives (X = F, CN or NMe₂) reported herein.

group (**Figure 1**).[23] This resulted in a WF shift from 5.2 to 4.1 eV upon SAM formation, highlighting the efficiency of the approach with respect to the dipole density and the orientation criteria for efficient WF engineering.[23]

As a critical intermediate in our synthesis involved a diketone, which was condensed to *ortho*-phenylenediamine to form the quinoxaline subunit of the diazatrypticene, a modular and versatile functionalization of the **DAT** tetrapod was deemed possible by utilizing any functionalized 1,2-diamine in the coupling step. In this work, as a representative example, we modulate the dipole of **DAT** by introducing several electron-donating and -withdrawing functional groups, allowing to tune the work function and surface energy of the gold substrate over a range of ≈1.0 eV, lowering it by a maximum of ≈1.3 eV with respect to the bare substrate.
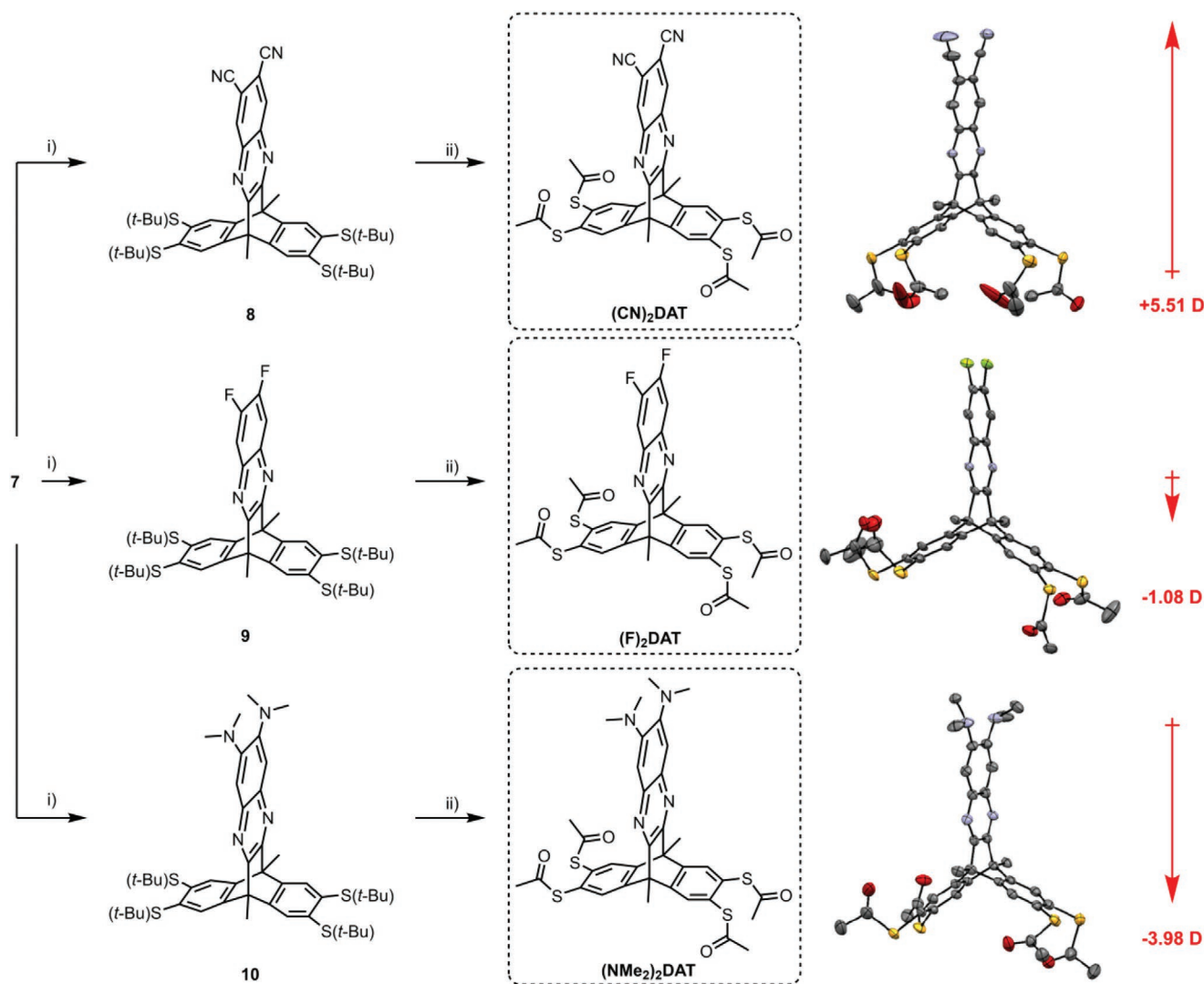
2. Results and Discussion

2.1. Synthesis of the Functionalized DATs

The synthesis of our **DAT** SAM precursors is portrayed in **Schemes 1** and **2**; the details are provided in the Supporting Information. In order to enable modular late-stage functionalization of the 1,2-diketone with dipolar head groups, we modified
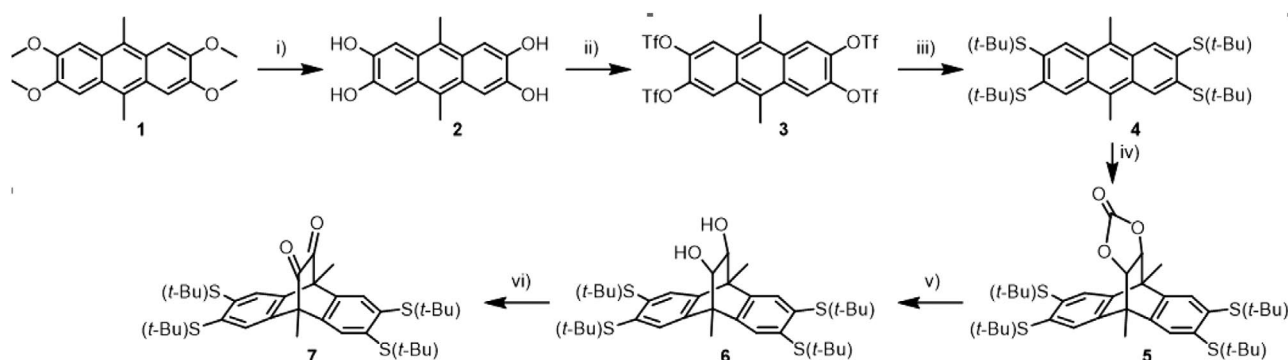
Scheme 1. Synthesis of the diketodibenzobarrelene building block **7**. Conditions: i) BBr₃, dichloromethane (DCM), −78 °C, 2 h to RT, 1 day, 90%; ii) Tf₂O, triethylamine, DCM, −78 °C to RT, 16 h, 36%; iii) Xantphos, Pd₂(dba)₃, Hünig's base, *tert*-BuSH, THF, 100 °C, 1 day, 80%; iv) vinylene carbonate, 1,2-dichlorobenzene, 140 °C, 3 days, 68%; v) NaOH, THF/H₂O, 80 °C, 1 h, 64%; vi) DMSO, TEA, TFFA, DCM, −78 °C, 150 min, 92%.

ADVANCED
SCIENCE NEWS
www.advancedsciencenews.com

ADVANCED
MATERIALS
TECHNOLOGIES
www.advmattechnol.de

Scheme 2. Synthesis of diazatriptycene SAM precursors (left) and their single crystal structures (right). Condensation conditions: i) corresponding diamine (CDCl$_3$ or MeOH) and HOAc, 100 °C, 30 min to 4 h. Yields: **8**: 58%, **9**: 58%, **10**: 52%. ii) Deprotection: toluene, AlCl$_3$, 16 h. Thioester formation: For **(CN)$_2$DAT**: toluene, triethylamine, AcCl, 0 °C, 5 min to RT, 30 min, 37%. For **(F)$_2$DAT**: DCM, TEA, AcCl, 0 °C 5 min, RT 30 min, 73%. For **(NMe$_2$)$_2$DAT**: NaHCO$_3$, (Ac)$_2$O, 15 min, 36%. Red arrows illustrate dipole moments calculated from the neutral tetrathioradicals using Hartree-Fock/6-31+G*.

our previously reported approach to **DAT**[23] such that the (protected) thiol anchoring groups were introduced as early and the dipole-modulating functional groups as lately as possible. Since phenyl thiols are prone to oxidation, we chose *tert*-butyl protecting groups because they are i) more resistant toward oxidation, ii) in contrast to acetyls are sufficiently stable with respect to basic hydrolysis and acidic condensation reaction media allowing a wide range of chemical postfunctionalization, and iii) can be transformed into the latter protecting group, whose efficiency for SAM formation on gold is well established.[22,37]

Demethylation of **1**, available on a 100 g scale via simple condensation of veratrole and acetaldehyde,[34] with BBr$_3$ yielded tetraol **2** in 90% yield.[38] **2** was triflated utilizing triflic anhydride under basic conditions (**3**, 36% yield) to enable subsequent fourfold Pd-catalyzed thiolation with *tert*-butylthiol furnishing **4** with a yield of 80%. Despite its high decomposition temperature, determined to be 233 °C via thermogravimetric

analysis/differential scanning calorimetry (TGA/DSC), partial debutylation was observed during Diels-Alder reaction of **4** with vinylene carbonate, even at a reaction temperature as low as 140 °C. Carbonate **5**, isolated with a yield of 68% after column chromatography, was then hydrolyzed with sodium hydroxide furnishing diol **6** (64%). A final Swern oxidation gave diketone **7** in excellent yields as a modular building block for the derivatization of SAM precursors on a gram scale.

Cyano, fluoro, or amino groups were introduced into our diazatrypticene SAM precursors via a two-step procedure (Scheme 2). Condensation of the respectively substituted phenylene diamines in acetic acid with a cosolvent (either DCM or MeOH) and **7** gave diazatrypticenes **8–10** in moderate yields (52–58%). Cleavage of the thioethers utilizing aluminum chloride, followed by thioesterification with acetyl chloride or acetic anhydride under basic conditions furnished **(CN)$_2$DAT**, **F$_2$(DAT)**, and **(NMe$_2$)$_2$DAT** in yields from 36% to 73%—the identity of

**ADVANCED
SCIENCE NEWS**

www.advancedsciencenews.com

**ADVANCED
MATERIALS
TECHNOLOGIES**

www.advmattechnol.de

each species was unambiguously confirmed via single crystal structure analysis. Substitution with electron-donating and -withdrawing groups modulates the calculated dipole moments of the tetrathioradicals, aligning with their C_2 symmetry axes, over a range of ≈9.5 D from −3.98 to +5.51 D, either pointing toward (amino, fluoro substituents, and nonfunctionalized) or away from the substrate (cyano functionalization).

2.2. SAM Preparation and Characterization

The **(CN)$_2$DAT**, **(F)$_2$DAT**, and **(NMe$_2$)$_2$DAT** SAMs, abbreviated together as **(X)$_2$DAT**, were prepared on Au(111) substrates using the procedure previously applied to the parent **DAT** monolayer.[23] The as-formed **(X)$_2$DAT** SAMs were characterized by infrared reflection absorption spectroscopy (IRRAS), near-edge X-ray absorption fine structure (NEXAFS) spectroscopy, X-ray photoelectron spectroscopy (XPS), and ultraviolet photoelectron spectroscopy (UPS). The broad range of analytical methods was necessary to analyze their quality, molecular orientation, binding configuration, packing density, and the WF change with respect to the bare substrate (for details on preparation and analysis see the Experimental Section).

2.2.1. IR Reflection-Absorption Spectroscopy

Infrared spectroscopy was used to prove the formation of the **(X)$_2$DAT** monolayers and to estimate the average molecular tilt angles from the molecule-specific vibration bands.[20,23] The angle of the molecular axis and the permanent dipole moment relative to the surface normal can be determined by comparing density functional theory (DFT) calculations with IR spectra. Two absorption bands with transition dipole moments parallel and orthogonal to the direction of the molecular dipole should be identified in the calculated and experimental spectra. Their intensity ratio in the spectra of the randomly distributed molecule and the monolayer on gold reveals the orientation of the molecules in the SAM.[23]
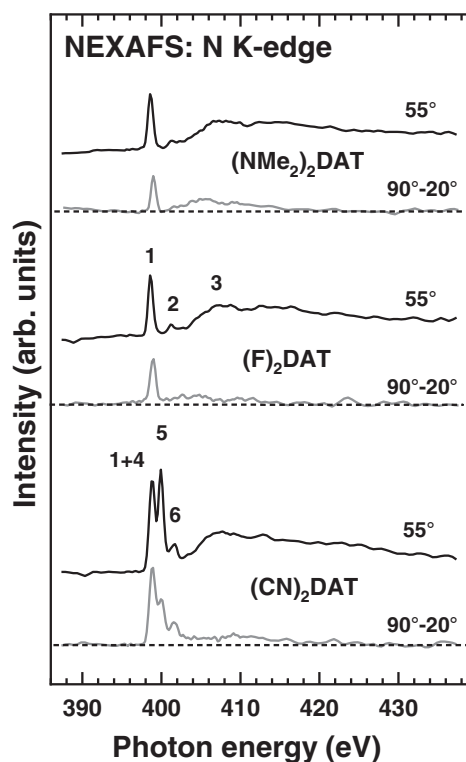
The IRRA spectra of the **(X)$_2$DAT** SAMs in the fingerprint range (800–1900 cm^{-1}) are shown in **Figure 2**a, along with the reference spectrum of the previously investigated unsubstituted **DAT** molecule.[23] Besides the characteristic molecular vibrations, the C=O stretching vibrations at 1700 cm^{-1} originating from the acetyl protection groups is identified. However, in comparison to the potassium bromide (KBr) powder spectrum (**Figure 3**c for **(NMe$_2$)$_2$DAT**), their intensities are strongly suppressed (≤0.3%), indicating a successful cleavage of the protection groups and hinting at the chemisorption of the molecules over the thiolate-gold anchors which is prerequisite for a successful SAM formation.

The IRRA spectrum of the **(CN)$_2$DAT** SAM (blue) contains the specific C≡N stretching vibrational mode at 2240 cm^{-1} for cyanides. For the **(F)$_2$DAT** SAM (green) the C−H bending vibrations of the quinoxaline terminus at 1250 and 1510 cm^{-1} are the strongest modes. As the transition dipole moments of the C−H vibrations are parallel to the molecular axis, the upright orientation of the platform on the gold surface is confirmed at a glance.
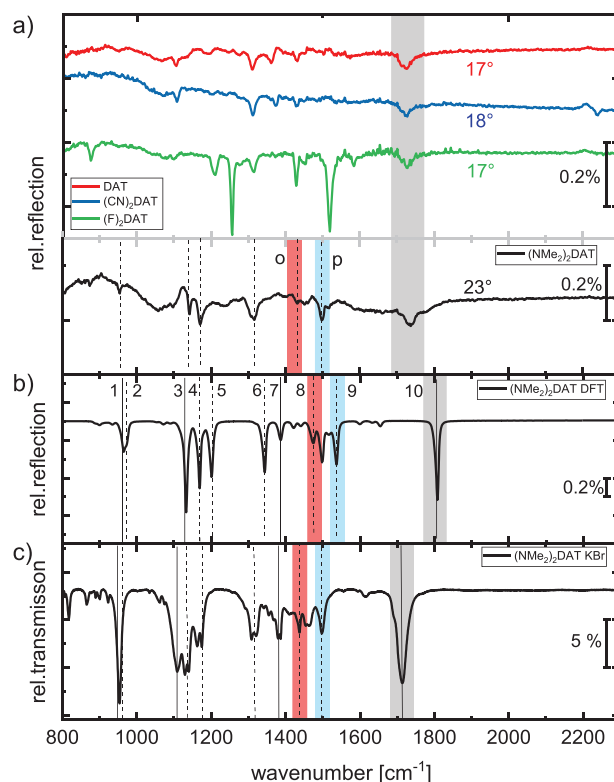
Figure 2. a) IRRA spectra of tetrapodal SAMs on gold; the derived average tilt angles are indicated at the respective curves (see text for details). b) DFT-simulated IRRA spectrum of a (NMe$_2$)$_2$DAT molecule on gold (B3LYP, 6-311+G(d,p); for details see the Supporting Information), and c) potassium bromide (KBr) powder spectrum of randomly oriented (NMe$_2$)$_2$DAT. Modes at 1430 cm^{-1} (red) and 1500 cm^{-1} (blue) are used for the estimation of the tilt angle of (NMe$_2$)$_2$DAT. The gray marked region is assigned to the ν(C=O) vibration of the acetyl protection group. The vertical dashed lines indicate characteristic molecular vibrations.

The tilt angles of the **(X)$_2$DAT** molecules in the SAMs on gold were calculated by comparing the intensities of orthogonal (o) and parallel (p) modes (with respect to the molecular axis, parallel to the molecular dipole). These modes have to be unambiguously assigned to the respective molecular vibrations and should not be influenced by contributions of the protecting acetates. The assignments of the most important absorption bands are shown exemplarily for **(NMe$_2$)$_2$DAT** (black) in Figure 2a–c with the measured IRRA spectrum, the simulated IRRA spectrum obtained from DFT calculations (see the Supporting Information for details) as well as the spectrum of the randomly oriented molecule in KBr powder. The modes are labeled with increasing numbers for increasing wavenumbers. The example of mode 1 already demonstrates the challenges of the assignment: Whereas this mode shows a strong oscillator strength in the isotropic KBr powder spectra, the respective peak is much weaker and broader in the simulated DFT spectrum. It refers, on the one hand, to the C−CH$_3$ stretching vibration of the acetyl protecting group and, on the other hand, to the parallel oriented C−H ring vibration of the upper quinoxaline ring, complicating a nonequivocal assignment. Modes 4–6 and 8–9 result from vibrations within the

**ADVANCED
SCIENCE NEWS**

www.advancedsciencenews.com

**ADVANCED
MATERIALS
TECHNOLOGIES**

www.advmattechnol.de

Figure 3. Representative N K-edge NEXAFS data for the **(X)₂DAT** SAMs including the spectra acquired at an X-ray incidence angle of 55° (black curves) and the difference between the spectra acquired at X-ray incidence angles of 90° and 20° (gray curves). Characteristic absorption resonances are numbered; see text for details and assignments. Horizontal dashed lines correspond to zero.

Table 1. Theoretical dipole moments and heights of the molecules in comparison to the layer thickness, orientation (average tilt angle) and work function shift (WFS).

DAT derivative	(CN)₂	(F)₂	(H)₂	(NMe₂)₂
Calculated dipole [D]	−5.51	1.08	2.71	3.98
Theoretical height [Å]	14.5	13.4	12.5	14.4
Layer thickness [Å ±0.1]	15.0	13.4	12.6	15.2
Orientation IRRAS [° ±5°]	18	17	17	23
Orientation NEXAFS [° ±5°]	22.5	25	14	23
Chemisorbed sulfur [%]	67	74	72	65
Packing density XPS [10¹⁴ molecules cm⁻²]	0.95	0.90	1.10	1.05
WF by UPS [eV ±0.1]	4.92	4.43	4.16	3.99
WFS by UPS [eV ±0.1]	−0.34	−0.76	−1.10	−1.20
WFS calculated [eV]	−0.37	−0.64	−1.10	−1.10

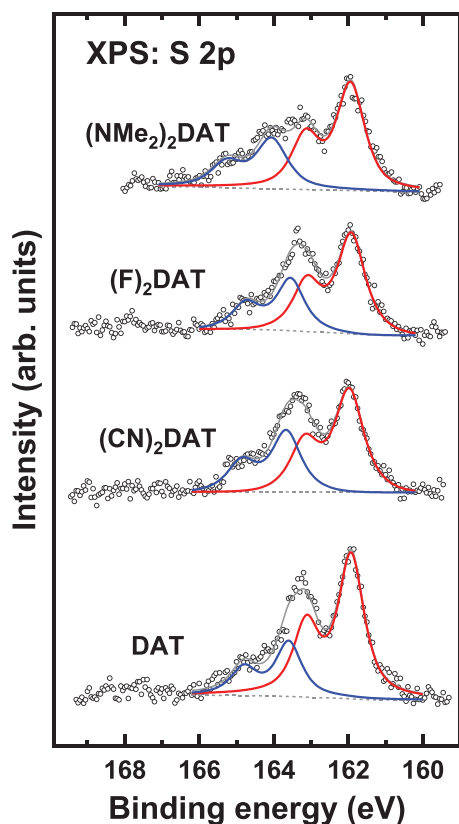### 2.2.2. NEXAFS Spectroscopy

The N K-edge NEXAFS spectra provide an alternative method to determine the tilt angles of the **(X)₂DAT** films. A representative data set is presented in Figure 3. It includes the spectra acquired at an X-ray incidence angle of 55°, exclusively representative of the electronic structure of the SAMs and the difference spectra (90°–20°), representing a fingerprint of the orientational order in the SAMs.[39] The 55° spectrum of the **(F)₂DAT** SAM solely contains resonances of the quinoxaline moiety and is similar to the analogous spectrum of the **DAT** monolayer.[23] It is dominated by the π^* resonance at ≈398.7 eV (1), accompanied by a second, much weaker π^* resonance at 401.3 eV (2), and a σ^* resonance at 406.7 eV (3), typical of quinoxalines[40] or pyrazines.[41–43] The 55° spectrum of the **(NMe₂)₂DAT** SAM is similar to that of the **(F)₂DAT** monolayer, as the terminal **(NMe₂)** groups only contribute to the σ^*-type resonances without influencing the most intense π^* resonance features. In contrast, the 55° spectrum of the **(CN)₂DAT** SAM is distinctly different. Herein, the resonances characteristics of the quinoxaline moiety (1) overlaps with those of the terminal nitrile groups, including a strong double resonance at ≈398.8 eV (4; π_1^*) and 399.8 eV (5; π_3^*) and a weaker resonance at 401.5 eV (6; π_4^*).[44]

The difference spectra of all substituted **DAT** SAMs exhibit positive peaks at the position of the characteristic π^* resonances. Considering that the transition dipole moments (TDMs) of the respective π^* orbitals are oriented perpendicular to the quinoxaline and nitrile moieties, this suggests an upright orientation of these moieties corresponding to a tetradentate or tridentate adsorption mode of the SAM forming molecules. A numerical evaluation of the entire sets of the NEXAFS spectra, based on the standard formalism for a vector-like orbital (the π^* resonances in our case), results in the average tilt angles of the quinoxaline moiety compiled in Table 1. Even though with certain deviations associated with the specific character and limited accuracy of both spectroscopic methods, the values derived from NEXAFS match the ones obtained via IR. The molecular inclination is independent from the substitution and all derivatives are oriented nearly orthogonal with respect to the surface.

whole molecule without the protecting group and thus are used for the calculation of the average tilt angle θ relative to the surface normal. The respective vibrational modes and their assignments for the cyanated and fluorinated derivatives are listed in Tables S4–S6 and Figures S26–S30 (Supporting Information). In case of **(NMe₂)₂DAT**, mode 8 unambiguously arises from a skeletal C—H wagging vibration with a transition dipole moment orthogonal (o) to the molecule's axis. Mode 9 belongs to a methyl bending vibration parallel (p) to the axis. From the ratio of the intensities of the absorbance of these two bands in the spectrum of the monolayer on gold (A_{SAM}) and the isotropic bulk spectrum of molecule (A_{Bulk}), the values of the average tilt angle, θ, were calculated by using the following relation

$$\theta = \arctan\sqrt{\frac{A_{SAM,o} \cdot A_{Bulk,p}}{2 A_{SAM,p} \cdot A_{Bulk,o}}} \qquad (1)$$

as applied in literature.[20,23] These values, compiled additionally in **Table 1**, amount to 18 ± 5°, 17 ± 5°, and 23 ± 5° for the **(CN)₂DAT**, **(F)₂DAT**, and **(NMe₂)₂DAT** SAMs, respectively, which is quite close to the tilt angle for the reference, nonsubstituted **DAT** monolayer (17 ± 5°),[23] indicating a nearly upright orientations. The substitution thus does not significantly affect the molecular inclination, confirming our assumption about the decoupling of the molecular anchoring and WF engineering for the DAT-based monolayers.

**ADVANCED
SCIENCE NEWS**

www.advancedsciencenews.com

**ADVANCED
MATERIALS
TECHNOLOGIES**

www.advmattechnol.de

2.2.3. Synchrotron-Based X-Ray Photoelectron Spectroscopy

The XPS data support the conclusion regarding the successful formation of the **(X)₂DAT** SAMs on Au(111). The C 1s spectra (see Figure S31 in the Supporting Information) exhibit a strong peak at ≈284.6 eV, associated with the platform and terminal phenyl moiety, and high binding energy features characteristic of the carbon atoms in the pyrazine ring (286.5 eV) as well as the carbon atoms bonded to fluorine (287.0 eV). The latter feature is only observed for the **(F)₂DAT** monolayer, underlining its identity. The N 1s spectra of all **(X)₂DAT** SAMs display a single peak, characteristic of the nitrogen atoms in the quinoxaline moiety and terminal groups (see Figure S31 in the Supporting Information). Its intensity is noticeably higher (by a factor of ≈2) for the **(CN)₂DAT** and **(NMe₂)₂DAT** SAMs as compared to the **(F)₂DAT** monolayer, corresponding to a twice as high nitrogen content. Information on the binding modes is gleaned from the S 2p XP spectra compiled in **Figure 4**. They represent a superposition of two individual doublets at ≈162.0 eV (S 2p$_{3/2}$) and ≈163.6 eV (S 2p$_{3/2}$), corresponding to thiolate bound to gold and unbound/weakly bound (e.g., physisorbed) thiols, respectively.[45] The portion of the potential anchoring groups covalently attached to the substrate varies from 63% to 73% over the series. Assuming an entirely monolayer character of the film,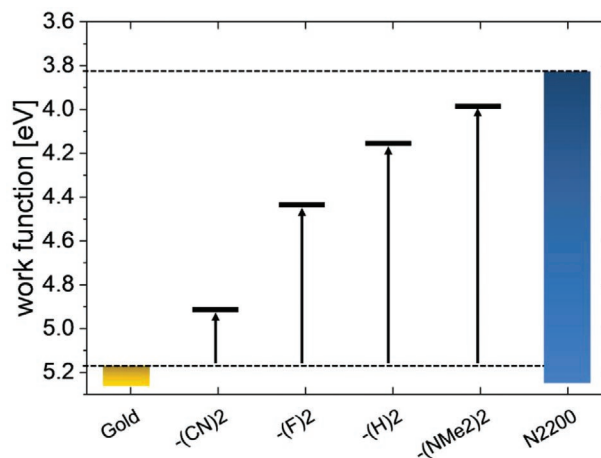 it follows that at least three of the four anchoring groups of each molecule are covalently bound to substrate. Alternatively, if we expect the presence of a certain amount of the physisorbed molecules in the film, the portion of the covalently bound anchors in the monolayer assembly could be even higher.

Based on the S 2p/Au 4f intensity ratio and using a SAM with a well-defined packing density as a reference,[23] the packing densities of the **(X)₂DAT** molecules in the monolayers were estimated (Table 1). They vary from 0.9×10^{14} to 1.05×10^{14} molecules cm^{-2}, close to the analogous experimental value for the **DAT** SAM (1.1×10^{14} molecules cm^{-2}).[23] As the molecular footprints of all derivatives are identical, we conclude a dense molecular packing for all monolayers. Based on the C 1s/Au 4f intensity ratio and using a SAM with a well-defined thickness as a reference, the effective thicknesses of the **(X)₂DAT** films were calculated (Table 1).[23] They vary from 13.5 to 15.2 Å, in agreement with the heights estimated from the crystal structures of the molecules and slightly exceeding that of the **DAT** SAM (12.6 Å)[23] due to incorporation of the dipolar groups.
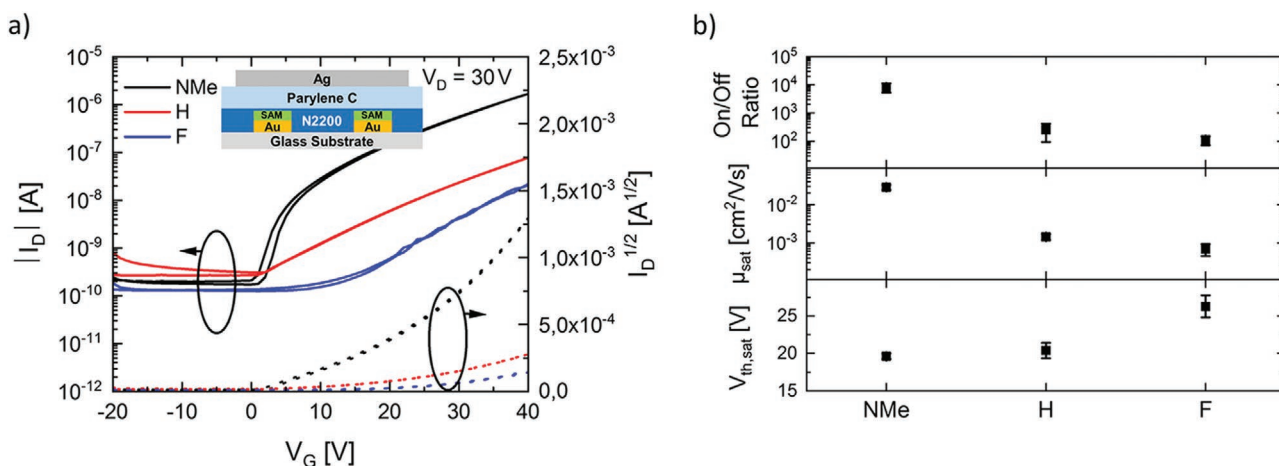
2.3. Work Function Tuning

The work function values for the **(X)₂DAT** and reference **DAT** SAMs are presented in **Figure 5** and compiled in Table 1 together with the average molecular tilt angles, the theoretical and XPS-derived SAM thickness, packing density, and the portion of the chemisorbed anchoring groups. For all SAMs, a reduction of the work function compared to the untreated gold electrode (≈5.2 eV) was observed, with the values varying between 4.92 and 3.99 eV. The measured work function shifts (WFS) follow the same trend as the calculated dipole strengths and thus confirm the design concept of **(X)₂DAT**.

The lowest work function of 3.99 eV was obtained with **(NMe₂)₂DAT**, as it exhibits the strongest dipole moment pointing toward the surface. Using the relation previously described,[23] we calculated the expected WFS by taking into account the experimentally derived tilt angles (for more details

Figure 4. S 2p XP spectra of the (X)₂-DAT and DAT (reference) films. The spectra are decomposed into two doublets assigned to the thiolate-gold bond (red solid line) and unbound sulfur (blue solid line); with the background indicated by the gray dashed line. The spectra were acquired at a primary photon energy of 350 eV.

Figure 5. Work functions of the as-prepared (≈5.2 eV) and SAM-functionalized gold substrates measured by UPS. The band gap of N2200[46] is schematically shown by the vertical blue bar.

**ADVANCED
SCIENCE NEWS**

www.advancedsciencenews.com

**ADVANCED
MATERIALS
TECHNOLOGIES**

www.advmattechnol.de

Figure 6. Parameters of the OFETs with SAM-modified electrodes. a) Representative transfer characteristics along with a schematic of an OFET; the curves are color-coded, the legend is provided in the plot; b) on/off ratios, field-effect mobilities, and threshold voltages of the OFETs. Shown are average values over at least three different devices with the standard deviation as statistical error.

see the Supporting Information). These WFSs are in good agreement with the experimental ones (see Table 1). With this finding, we demonstrate that our tetrapodal system offers the advantage of work function engineering by the variation of dipolar head groups at the diazatriptycene scaffold.

2.4. OFETs with SAM-Treated Gold Electrodes

The **DAT**-based SAMs were applied for electrostatic electrode engineering in proof-of-concept OFET devices.[15,16] For this purpose, source and drain gold electrodes, supported by a glass substrate, were immersed into the corresponding SAM solutions before depositing the n-type polymeric semiconductor **N2200**.[46] The subsequent coating with a Parylene C dielectric and a silver gate electrode afforded bottom contact, top gate OFETs (**Figure 6**). For **(CN)$_2$DAT** no working transistor was achieved—in this case, the energetic mismatch (Schottky-barrier) between the work function of the SAM-modified gold electrode (4.92 eV) and the LUMO of **N2200** (3.84 eV)[46] corresponded to a too high electron injection barrier. A further decrease of the WF of the gold electrodes by **DAT** (WF = 4.43 eV) and **(NMe$_2$)$_2$DAT** (WF = 3.99 eV), corresponding to the gradual lowering of the Schottky-barrier, resulted in progressive increase of the drain current, with a maximum value observed for the **(NMe$_2$)$_2$DAT** case. This relationship was furthermore reflected in the on/off ratio of the transistors as well as in their field-effect mobilities: With a decreasing Schottky barrier, the on/off ratio increased from $\approx 10^2$ for **DAT** and **(F)$_2$DAT** to 10^4 for **(NMe$_2$)$_2$DAT**, whereas the field effect mobilities increased from nearly 10^{-3} to above 10^{-2} V s cm^{-2}. The threshold voltage was also slightly improved, going from 30 to 20 V.

Overall, the performance of the OFETs correlated well with the electrostatic properties of the gold electrodes tailored by the **(X)$_2$DAT** SAMs. The general behavior of the OFETs can be rationalized in terms of energy matching between the work function of these electrodes and the electron affinity (EA) of the test semiconductor.

3. Conclusions

We demonstrated that the tetrapodal, thio-functionalized diazatrypticene **DAT**, capable of forming SAMs on coinage metal substrates, can be easily substituted with dipolar head groups, establishing this system as a useful tool for electrostatic engineering of surfaces and interfaces in context of organic electronics. Both electron-donating and electron-withdrawing groups were modularly introduced via attachment of differently functionalized 1,2-phenylenediamines to the common dibenzobarrelene scaffold by two-steps condensation reaction. Significantly, the parameters of the **DAT**-based SAMs, such as the packing density, anchoring configuration, and molecular inclination were only marginally affected by the substitution, underlining further the robustness and flexibility of the system. The work function of the SAM-modified gold substrates correlated well with the molecular dipole, with the work function shifts being well reproduced by the model calculations relying on the specific parameters of the monolayers determined within their characterization. The performance of the dipolar, **DAT**-based SAMs was demonstrated by their applications in OFETs. The engineering of the source and drain electrodes furnished a good correlation between the Schottky-barrier at the electrode–organic semiconductor interface and the performance of the devices. Our tetrapodal diazatrypticene system stands out among other multipods as it simultaneously meets all of the criteria for versatile and effective surface engineering in terms of a small footprint to guarantee a high surface coverage, controlled and reproducible spatial orientation, stability, and ease of functionalization. The dipolar head groups chosen in this study represent only a small fraction of possible substitution patterns since any other functional head groups can be used as well, which makes the **DAT**-based SAMs a versatile, flexible, and useful system for a variety of applications, ranging from basic interfacial engineering to sensor fabrication, biotechnology, and surface-anchored molecular machines. Another possible modification includes the introduction of different anchoring groups, such as phosphonic or carboxylic acids,

etc., to allow work-function engineering of popular organic photovoltaic materials like indium tin oxide and aluminum, thus, extending the application range of the **DAT**-based SAMs to organic photovoltaics and light-emitting diodes.

4. Experimental Section

Preparation of SAMs: All solvents were obtained from commercial suppliers and used without further purification. The gold substrates were prepared as reported in ref. [47] by successive evaporation of a 5 nm thin titanium adhesion layer and a 180 nm thick gold layer on a precleaned silicon substrate. The SAM preparation was performed under an inert nitrogen atmosphere in a glovebox. The SAM precursors were first dissolved in tetrahydrofuran (anhydrous, ≥99.9%, inhibitor-free, Sigma-Aldrich), mixed with methanol (anhydrous, 99.8%, Sigma-Aldrich) in a 3:1 volumetric ratio, and subsequently stirred for 30 min at 30 °C. Clean gold substrates were then immersed in the resulting 25×10^{-6} M DAT solutions (3 mL) for 10 min and methanolic ammonia solution (1 M, 1 mL, Sigma-Aldrich) was added as a cleaving agent to deprotect the acetyl protection groups and furnish the free thiols, which could then covalently bind to gold to form a monolayer. Subsequently, to remove possible contaminants and physisorbed material, the samples were cleaned in an ultrasonic bath, washed with pure methanol, and sonicated in methanol and THF in ambient in a fume hood for each 10 min. Finally, after drying under nitrogen, the samples were transferred back into the glovebox and annealed at 150 °C for 1.5 h.

IRRAS: The measurements were performed using a Vertex 80v (Bruker) Fourier-transform (FT) IR spectrometer equipped with a nitrogen-cooled mercury cadmium telluride detector. The spectra were measured with p-polarized light and averaged over about 600 scans. The energy resolution was estimated at 2 cm^{-1}. The raw spectra of the SAMs were divided by a reference spectrum of a clean gold substrate, thus giving the relative reflectance R of the monolayer. The tilt angle analysis was carried out according to the established procedure, the efficiency of which has been demonstrated previously.[23,47,48] For simulating the DFT spectrum of an isotropic molecule on gold, the simulation software package SCOUT[49] was used.

Synchrotron-Based XPS: The measurements were carried out at the high energy spherical grating monochromator (HE-SGM) beamline (bending magnet) of the synchrotron storage ring BESSY II in Berlin, Germany, using a custom-made experimental station equipped with a Scienta R3000 electron energy analyzer. The synchrotron light served as the primary X-ray source. The energy resolution was ≈0.3 eV at a photon energy of 350 eV. The experiments were performed at room temperature and in ultrahigh vacuum (a base pressure of 10^{-9} mbar). The binding energy (BE) scale of the spectra was referenced to the Au 4f$_{7/2}$ emission at 84.0 eV.[50] The spectra were fitted by symmetric Voigt functions and either a linear or Shirley-type background. To fit the S 2p$_{3/2,1/2}$ doublets, two peaks with the same full width at half-maximum (fwhm), a standard spin-orbit splitting of ≈1.2 eV (verified by a fit), and a branching ratio of 2 (S 2p$_{3/2}$/S 2p$_{1/2}$) were used. The effective thicknesses of the SAMs and their packing densities were calculated using standard procedures, based on the C1s/Au4f and S2p/Au4f intensity ratios, respectively.[51,52] The spectrometer-specific coefficients were determined by using a hexadecanethiolate SAM on Au(111) as a reference, relying on its well-known thickness and packing density.[53]

NEXAFS Spectroscopy: The spectra were acquired at the same beamline and the experimental station as the XP ones. They were measured at the carbon and nitrogen K-edges in the partial electron yield (PEY) mode with retarding voltages of −150 and −300 V, respectively, but only the N–K-edge data are presented. Linearly polarized synchrotron light with a polarization factor of ≈89% was used as the primary X-ray source. The incidence angle of the X-rays was varied between the normal (90°) and grazing (20°) incidence geometry to monitor the linear dichroism reflecting the molecular orientation in the SAMs.[39] The energy resolution was ≈0.3 eV at the C K-edge and ≈0.45 eV at the N

K-edge. The photon energy scale was referenced to the pronounced π^* resonance of HOPG at 285.38 eV.[54] The spectra were corrected for the PE dependence of the incident photon flux and reduced to the standard form with zero intensity in the pre-edge region and the unity jump in the far post-edge region.

Work Function Determination by UPS: The photoelectron spectroscopic (PES) measurements were performed using the VersaProbe II of PHI equipped with a monochromatized Al Kα X-ray ($h\nu$ = 1486 eV) source and an Omicron HIS 13 helium discharge lamp (HeI: $h\nu$ = 21.22 eV) as excitation sources for XPS and UPS. Secondary electron edges were calibrated via the work function of in situ sputter-cleaned Ag foil determined by UPS. Here, the Ag UP spectrum was referenced to its Fermi level position. The base pressure of the measuring chamber during all experiments was kept in the 10^{-9} mbar range. The take-off angle was 90°.

Fabrication of OFETs: PNDI(2OD)2T (N2200), purchased from Ossila, was dissolved in chlorobenzene at a concentration of 10 g L^{-1} and stirred at 50 °C for several hours. The solution was spin coated with at 1000 RPM for 60 s and an acceleration of 500 RPM s^{-1} on glass substrates with thermally evaporated gold contacts for *IV*-measurements. The resulting thicknesses of the N2200 film, representing the active layer, was 60 nm. The thickness of the contacts was 60 nm, the channel length and width were 20 μm and 1 mm, respectively. Afterward, a ≈565 nm thick film of poly(chloro-*p*-xylylene) (Parylene C) was deposited as a gate dielectric on top of the active layer by chemical vapor deposition in a commercially available PDS2010 coating system (Specialty Coating Systems). Finally, silver gate electrode was thermally deposited on top of the dielectric.

Electrical Measurements: All electrical measurements were performed in air at room temperature and in the dark using a Semiconductor Parameter Analyzer 4155C by Agilent Technologies. Several samples were fabricated and representative results are shown. For reliability, at least three different samples were considered in each particular case providing standard deviation as statistical error. Conductivities were calculated from the *IV*-measurements on the corresponding films used in the OFETs. Transfer characteristics were measured by device operation in accumulation mode. Field-effect mobilities in the saturated regime were then calculated from the transconductance according to the formula $\mu_{sat} = \left(\frac{2L}{WC}\right) \cdot \left(\frac{\partial \sqrt{I_D}}{\partial V_G}|_{V_D = const.}\right)^2$ as described elsewhere.[55] However, in view of the specific shape of our transfer curves, the derived mobility values should be considered as tentative only.[56] Threshold voltages were evaluated through the intersection of the extrapolation of $\sqrt{I_D}$ in the saturation region with the axis of abscissa as described elsewhere as well.[57]

Dipole Calculations: The molecular dipole moments, μ, of the **(X)$_2$DAT** molecules were calculated from the neutral tetrathiole radical, using Hartree–Fock method and basis set 6-31+G*.

Supporting Information

Supporting Information is available from the Wiley Online Library or from the author.

Acknowledgements

[1] C. Vericat, M. E. Vela, G. Corthey, E. Pensa, E. Cortés, M. H. Fonticelli, F. Ibañez, G. E. Benitez, P. Carro, R. C. Salvarezza, *RSC Adv.* **2014**, *4*, 27730.

[2] A. S. Sizov, A. A. Trul, V. Chekusova, O. V. Borshchev, A. A. Vasiliev, E. V. Agina, S. A. Ponomarenko, *ACS Appl. Mater. Interfaces* **2018**, *10*, 43831.

[3] J. F. Stoddart, *Acc. Chem. Res.* **2001**, *34*, 410.

[4] V. Ferri, M. Elbing, G. Pace, M. D. Dickey, M. Zharnikov, P. Samorì, M. Mayor, M. A. Rampi, *Angew. Chem., Int. Ed.* **2008**, *47*, 3407.

[5] L. Motiei, M. Lahav, D. Freeman, M. E. Van der Boom, *J. Am. Chem. Soc.* **2009**, *131*, 3468.

[6] R. A. Marcus, *Rev. Mod. Phys.* **1993**, *65*, 599.

[7] A. Salomon, D. Cahen, S. Lindsay, J. Tomfohr, V. B. Engelkes, C. D. Frisbie, *Adv. Mater.* **2003**, *15*, 1881.

[8] W. Du, T. Wang, H. S. Chu, L. Wu, R. Liu, S. Sun, W. K. Phua, L. Wang, N. Tomczak, C. A. Nijhuis, *Nat. Photonics* **2016**, *10*, 274.

[9] S. Hietzschold, S. Hillebrandt, F. Ullrich, J. Bombsch, V. Rohnacher, S. Ma, W. Liu, A. Kö, W. Jaegermann, A. Pucci, W. Kowalsky, E. Mankel, S. Beck, R. Lovrincic, *ACS Appl. Mater. Interfaces* **2017**, *9*, 39821.

[10] X. Cheng, Y.-Y. Noh, J. Wang, M. Tello, J. Frisch, R.-P. Blum, A. Vollmer, J. P. Rabe, N. Koch, H. Sirringhaus, *Adv. Funct. Mater.* **2009**, *19*, 2407.

[11] U. Zschieschang, F. Ante, M. Schlörholz, M. Schmidt, K. Kern, H. Klauk, *Adv. Mater.* **2010**, *22*, 4489.

[12] K. P. Pernstich, S. Haas, D. Oberhoff, C. Goldmann, D. J. Gundlach, B. Batlogg, A. N. Rashid, G. Schitter, *J. Appl. Phys.* **2004**, *96*, 6431.

[13] S. Kobayashi, T. Nishikawa, T. Takenobu, S. Mori, T. Shimoda, T. Mitani, H. Shimotani, N. Yoshimoto, S. Ogawa, Y. Iwasa, *Nat. Mater.* **2004**, *3*, 317.

[14] S. K. Possanner, K. Zojer, P. Pacher, E. Zojer, F. Schürrer, *Adv. Funct. Mater.* **2009**, *19*, 958.

[15] M. Jesper, M. Alt, J. Schinke, S. Hillebrandt, I. Angelova, V. Rohnacher, A. Pucci, U. Lemmer, W. Jaegermann, W. Kowalsky, T. Glaser, E. Mankel, R. Lovrincic, F. Golling, M. Hamburger, U. H. F. Bunz, *Langmuir* **2015**, *31*, 10303.

[16] M. Alt, M. Jesper, J. Schinke, S. Hillebrandt, P. Reiser, T. Rödlmeier, I. Angelova, K. Deing, T. Glaser, E. Mankel, W. Jaegermann, A. Pucci, U. Lemmer, U. H. F. Bunz, W. Kowalsky, G. Hernandez-Sosa, R. Lovrincic, M. Hamburger, *Adv. Funct. Mater.* **2016**, *26*, 3172.

[17] D. Alberga, G. F. Mangiatordi, A. Motta, O. Nicolotti, G. Lattanzi, *Langmuir* **2015**, *31*, 10693.

[18] S. A. Paniagua, A. J. Giordano, O. L. Smith, S. Barlow, H. Li, N. R. Armstrong, J. E. Pemberton, J.-L. Brédas, D. Ginger, S. R. Marder, *Chem. Rev.* **2016**, *116*, 7117.

[19] J. C. Love, L. A. Estroff, J. K. Kriebel, R. G. Nuzzo, G. M. Whitesides, *Chem. Rev.* **2005**, *105*, 1103.

[20] F. S. Benneckendorf, S. Hillebrandt, F. Ullrich, V. Rohnacher, S. Hietzschold, D. Jä, J. Freudenberg, S. Beck, E. Mankel, W. Jaegermann, A. Pucci, U. H. F. Bunz, K. Mü, *J. Phys. Chem. Lett.* **2018**, *9*, 3731.

[21] A. Petritz, M. Krammer, E. Sauter, M. Gärtner, G. Nascimbeni, B. Schrode, A. Fian, H. Gold, A. Cojocaru, E. Karner-Petritz, R. Resel, A. Terfort, E. Zojer, M. Zharnikov, K. Zojer, B. Stadlober, *Adv. Funct. Mater.* **2018**, *28*, 1804462.

[22] B. de Boer, A. Hadipour, M. M. Mandoc, T. van Woudenbergh, P. W. M. Blom, *Adv. Mater.* **2005**, *17*, 621.

[23] F. S. Benneckendorf, V. Rohnacher, E. Sauter, S. Hillebrandt, M. Münch, C. Wang, S. Casalini, K. Ihrig, S. Beck, D. Jänsch, J. Freudenberg, W. Jaegermann, P. Samorì, A. Pucci, U. H. F. Bunz, M. Zharnikov, K. Müllen, *ACS Appl. Mater. Interfaces* **2020**, *20*, 6565.

[24] Z. Q. Li, J. H. Tang, Y. W. Zhong, *Chem. - Asian J.* **2019**, *14*, 3119.

[25] J. Hu, D. L. Mattern, *J. Org. Chem.* **2000**, *65*, 2277.

[26] T. Weidner, A. Krämer, C. Bruhn, M. Zharnikov, A. Shaporenko, U. Siemeling, F. Träger, *Dalton Trans.* **2006**, 2767.

[27] M. Lindner, M. Valášek, J. Homberg, K. Edelmann, L. Gerhard, W. Wulfhekel, O. Fuhr, T. Wächter, M. Zharnikov, V. Kolivoška, L. Pospíšil, G. Mészáros, M. Hromadová, M. Mayor, *Chem. - Eur. J.* **2016**, *22*, 13218.

[28] R. Sakamoto, Y. Ohirabaru, R. Matsuoka, H. Maeda, S. Katagiri, H. Nishihara, *Chem. Commun.* **2013**, *49*, 7108.

[29] S. Wagner, F. Leyssner, C. Kördel, S. Zarwell, R. Schmidt, M. Weinelt, K. Rück-Braun, M. Wolf, P. Tegeder, *Phys. Chem. Chem. Phys.* **2009**, *11*, 6242.

[30] M. Valášek, K. Edelmann, L. Gerhard, O. Fuhr, M. Lukas, M. Mayor, *J. Org. Chem.* **2014**, *79*, 7342.

[31] Z. Cao, J. S. Derrick, J. Xu, R. Gao, M. Gong, E. M. Nichols, P. T. Smith, X. Liu, X. Wen, C. Copéret, C. J. Chang, *Angew. Chem.* **2018**, *130*, 5075.

[32] G. Erbland, S. Abid, Y. Gisbert, N. Saffon-Merceron, Y. Hashimoto, L. Andreoni, T. Guérin, C. Kammerer, G. Rapenne, *Chem. - Eur. J.* **2019**, *25*, 16328.

[33] F. Ishiwari, G. Nascimbeni, E. Sauter, H. Tago, Y. Shoji, S. Fujii, M. Kiguchi, T. Tada, M. Zharnikov, E. Zojer, T. Fukushima, *J. Am. Chem. Soc.* **2019**, *141*, 5995.

[34] J. Rochford, D. Chu, A. Hagfeldt, E. Galoppini, *J. Am. Chem. Soc.* **2007**, *129*, 4655.

[35] V. Kaliginedi, H. Ozawa, A. Kuzume, S. Maharajan, I. V. Pobelov, N. H. Kwon, M. Mohos, P. Broekmann, K. M. Fromm, M. A. Haga, T. Wandlowski, *Nanoscale* **2015**, *7*, 17685.

[36] B. Baisch, D. Raffa, U. Jung, O. M. Magnussen, C. Nicolas, J. Lacour, J. Kubitschke, R. Herges, *J. Am. Chem. Soc.* **2009**, *131*, 442.

[37] A. Ulman, *Chem. Rev.* **1996**, *96*, 1533.

[38] H. Hu, M. P. Singh, G. S. Baghel, G. W. Dye, D. L. Gerlach, T. P. Vaid, *ChemistrySelect* **2016**, *1*, 2163.

[39] J. Stöhr, *NEXAFS Spectroscopy, Springer Series in Surface Sciences*, Vol. 25, Springer, Berlin, Germany **2003**.

[40] G. Richard, A. Cros, Y. Mathey, G. Tourillon, C. Laffon, Y. Parent, *J. Phys. IV* **1993**, *03*, C7.

[41] R. Dudde, K. H. Frank, E. E. Koch, *J. Electron Spectrosc. Relat. Phenom.* **1988**, *47*, 245.

[42] R. Dudde, M. L. M. Rocco, E. E. Koch, S. Bernstorff, W. Eberhardt, *J. Chem. Phys.* **1989**, *91*, 20.

[43] H.-K. Lee, J. Park, I. Kim, H.-D. Kim, B.-G. Park, H.-J. Shin, I.-J. Lee, A. P. Singh, A. Thakur, J.-Y. Kim, *J. Phys. Chem. C* **2012**, *116*, 722.

[44] M. Zharnikov, *J. Electron Spectrosc. Relat. Phenom.* **2015**, *200*, 160.

[45] M. Zharnikov, *J. Electron Spectrosc. Relat. Phenom.* **2010**, *178–179*, 380.

[46] L. Gao, Z. G. Zhang, L. Xue, J. Min, J. Zhang, Z. Wei, Y. Li, *Adv. Mater.* **2016**, *28*, 1884.

[47] M. Alt, J. Schinke, S. Hillebrandt, M. Hänsel, G. Hernandez-Sosa, N. Mechau, T. Glaser, E. Mankel, M. Hamburger, K. Deing, T. Glaser, E. Mankel, W. Jaegermann, A. Pucci, U. Lemmer, U. H. F. Bunz, W. Kowalsky, G. Hernandez-Sosa, R. Lovrincic, M. Hamburger, *ACS Appl. Mater. Interfaces* **2014**, *6*, 20234.

[48] M. Tzschoppe, C. Huck, B. Günther, M. Matthiesen, C. Ulrich, J. N. Rose, A. Butkevich, V. Rohnacher, L. H. Gade, J. Zaumseil, A. Pucci, *J. Phys. Chem. C* **2020**, *124*, 769.

[49] W.Theiss, SCOUT—Software Package for Optical Spectroscopy, WTheiss Hardware and Software, Tucson, AZ 85749, USA.

[50] J. F. Moulder, W. E. Stickle, P. E. Sobol, K. D. Bomben, *Handbook of X-ray Photoelectron Spectroscopy* (Ed: J. Chastian), Perkin-Elmer Corp., Eden Prairie, USA **1992**.

[51] J. Thome, M. Himmelhaus, M. Zharnikov, M. Grunze, *Langmuir* **1998**, *14*, 7435.

[52] E. Sauter, G. Nascimbeni, D. Trefz, S. Ludwigs, E. Zojer, F. Von Wrochem, M. Zharnikov, *Phys. Chem. Chem. Phys.* **2019**, *21*, 22511.

[53] F. Schreiber, *Prog. Surf. Sci.* **2000**, *65*, 151.

[54] P. E. Batson, *Phys. Rev. B* **1993**, *48*, 2608.

[55] D. Choi, P.-H. Chu, M. McBride, E. Reichmanis, *Chem. Mater.* **2015**, *27*, 4167.

[56] E. G. Bittle, J. I. Basham, T. N. Jackson, O. D. Jurchescu, D. J. Gundlach, *Nat. Commun.* **2016**, *7*, 10908.

[57] C. Bock, D. V. Pham, U. Kunze, D. Käfer, G. Witte, C. Wöll, *J. Appl. Phys.* **2006**, *100*, 114517.